A COMPRESSED SENSING-BASED PAN-SHARPENING USING JOINT DATA FIDELITY AND BLIND BLURRING KERNEL ESTIMATION

Yiyong Jiang[1], *Liqin Chen*[1], *Wei Wang*[2], *Xinghao Ding*[1,3*] *and Yue Huang*[1,3*]

[1]Department of Communication Engineering, Xiamen University, Xiamen, China
[2]Department of Electronic Engineering, Xiamen University, China
[3]Key Lab of Underwater Acoustic Communication and Marine Information Technology, Ministry of Education, Xiamen, China
E-mail: dxh@xmu.edu.cn

ABSTRACT

Pan-sharpening is an approach that fuse low resolution multispectral (LRMS) images with a high spatial detail of panchromatic (PAN) image to obtain the high resolution multispectral (HRMS) images. In this paper, we present a compressed sensing-based pan-sharpening method that include joint data fidelity and blind blurring kernel estimation. The joint data fidelity contain following three fidelity terms: (1) the LRMS images could be the decimated form of the HRMS images by convolving a blurring kernel, (2) the gradient of HRMS images in the spectrum direction could be proximity to those of the LRMS images, (3) the high frequency part of linear combination of HRMS image bands is approximate to the corresponding parts of the PAN image. Different from other methods which simply apply average blurring kernel for pan-sharpening, a blind deconvolution algorithm is introduced to estimate the blurring kernel from different satellites respectively. We also include a novel anisotropic total variation (TV) prior term to better reconstruct the image edges. The alternating direction method of multipliers (ADMM) is used to solve the proposed model efficiently. Finally, a Pléiades satellite image is employed to demonstrate that the proposed method achieve effective and efficient results simultaneously compared with other existing methods.

Index Terms— Pan-sharpening, image fusion, total variation, remote sensing, blurring kernel estimation

1. INTRODUCTION

Remote sensor data provided by satellites such as QuickBird, Pléiades, IKONOS, .etc, usually contain both multispectral (MS) images and a panchromatic (PAN) image respectively. The MS images contain plentiful spectral information, but always have lower spatial resolution. Panchromatic (PAN) image possesses high spatial detail information, but it is only a grayscale image. Owing to current remote sense technique limits, images come from satellite sensors cannot contain both high spectral and high spatial resolution [1]. However, spectral information and high spatial detail information are both desired in one image. So pan-sharpening methods are increasingly desired in remote sensing application.

Up to now, various pan-sharpening approaches have been presented. The most common ones are projection-substitution-based methods and they assume that the PAN image is equivalent to a linear structural component of the HRMS images [2]. Among them, the principal component analysis (PCA) [3], the Brovey transform [4] and intensity-hue-saturation(IHS) [5][6] are the most popular ones because of their relatively straightforward implement and fast computation. Fusion results of the three mentioned methods have good spatial details. However, since the spectral range of PAN image is not correspond to that of the HRMS images covered and the gray value between PAN and HRMS images is significant difference, tending to produce spectral distortion when use the methods mentioned above [7].

Recently, the inverse-problem-based methods for pan-sharpening applications become increasingly popular [2]. The most popular example is the compressed sensing(CS) based method [2][8][9], which uses sparse regularization with respect to patch-level dictionary learning. However, those previous CS-based methods have some common limitations, e.g., inefficiency, since their dictionary learning is time-consuming and they focus on using prior of images, paying less attention upon the effect of image fidelity term. Moreover, they assume that the blurring kernel between different satellites is constant, this is not consistent with the practical application. [10] is another inverse-problem-based approach based on variational framework, but it lack of prior knowledge of HRMS images that it leaves the result quality to improve.

In this paper, we propose a CS-based pan-sharpening

The project is supported by the National Natural Science Foundation of China(No. 30900328, 61172179, 61103121, 71103150, 81301278), the Natural Science Foundation of Fujian Province of China (No. 2012J05160), the National Key Technology R&D Program (2012BAI07B06), the Fundamental Research Funds for the Central Universities (No. 2011121051, 2013121023).

approach that uses the joint data fidelity and blind blurring kernel estimation. Compared with the previous CS-based pan-sharpening methods, the proposed model has the following characteristics:

1. It uses the joint data fidelity that overall consider the fidelity between HRMS images and LRMS images, the gradient in the spectrum direction of HRMS images and LRMS images, HRMS images and PAN image in high frequency part.

2. We consider that it is more reasonable for actual application to estimate the blurring kernel from different satellites than simply applying average blurring kernel for pan-sharpening.

3. We include a novel anisotropic TV as a prior term which is imposed to better reconstruct the edges and the alternating direction method of multipliers (ADMM) [11] helps to perform an efficient optimization procedure.

2. PROPOSED PAN-SHARPENING MODEL

We write the objective function for our model as follows:

$$L(x_1, x_2, x_3, x_4) = \sum\nolimits_i f(x_i, y_i^{MS}, y^P) + \frac{\lambda}{2} \sum\nolimits_i \|x_i\|_{TV} \quad (1)$$

where $f(x_i, y_i^{MS}, y^P)$ is the joint date fidelity term and $\|x_i\|_{TV}$ is the anisotropic TV prior term. y_i^{MS} and x_i represent the ith band of the LRMS images and HRMS images, respectively. $i = 1, 2 \cdots, N$, N is the number of bands of the MS images. y^P denotes the PAN image. λ is the weight parameter.

2.1. Joint Date Fidelity

The joint data fidelity can be written as follows:

$$f(x_i, y^{MS}, y^P) = \frac{v_1}{2} f_1(x_i, y_i^{MS}) + \frac{v_2}{2} f_2(x_i, y_i^{MS}) + \frac{v_3}{2} f_3(x_i, y^P) \quad (2)$$

where $f_1(x_i, y_i^{MS})$, $f_2(x_i, y_i^{MS})$ and $f_3(x_i, y^P)$ constitute our joint data fidelity. The regularization parameters v_1, v_2 and v_3 are used to balance the contribution of each fidelity term in our model.

The first fidelity term $f_1(x_i, y_i^{MS}) = \|k * x_i - y_i^{MS}\|_2^2$ assume that the LRMS image could be the decimated form of the HRMS images by convolving with the blurring kernel k. In this paper, the blurring kernel k is obtained by estimation according to the blurring characteristic of different satellite respectively. Compared with other method which apply average blurring kernel for pan-sharpening, this is considered more reasonable in accordance with the actual application. The blurring kernel estimation process is introduced in Section 3.

The fidelity term $f_2(x_i, y_i^{MS}) = \|D_s \boldsymbol{x_i} - D_s \boldsymbol{y_i^{MS}}\|_2^2$ forces a proximity between HRMS images and LRMS images of the gradient part in the spectrum direction. Since MS images are discrete in spectrum direction, the gradient $D_s \boldsymbol{x_i}$ can be expressed as the following difference scheme [10],

$$D_s \boldsymbol{x_i} = \{x_i - x_{i+1}, \quad i = 1, \cdots, N-1\}$$

Apparently, the above equation is approximately equivalent to

$$x_i - x_n = y_i^{MS} - y_n^{MS}, \quad i = 1, \cdots, N-1, \quad n = i+1, \cdots, N$$

Therefore, the term $f_2(x_i, y_i^{MS})$ can be rewrite as

$$f_2(x_i, y_i^{MS}) = \| \sum_{n=i+1}^{N} |x_i - x_n - (y_i^{MS} - y_n^{MS})| \|_2^2, \quad i = 1, \cdots, N-1. \quad (3)$$

The last fidelity term $f_3(x_i, y^P) = \|G_i(\sum_{b=1}^{N} \omega_b x_b - y^P)\|_2^2$ uses the PAN image to provide the spatial information. G_i is a high-pass filter kernel which aims to enforcing high frequency of the PAN image and the HRMS images while minimizing spectral distortion. The ω_b is the trade-off parameters which satisfies $\sum_{b=1}^{N} \omega_b = 1$. Most pan-sharpening models do this by incorporating a squared error term $\sum_i \| \sum_{b=1}^{N} \omega_b x_b - y^P \|_2^2$ [2]. But this pixel-level relationship between PAN image and HRMS images is not very exact in practice, because the band covers and pixel value of them are different. However, PAN image and HRMS images have the similar high frequency information as shown in Fig.1. We can find that the high frequency edge details between PAN image and HRMS images are more similar than that of their pixel value.

2.2. Prior term: anisotropic TV

Since the anisotropic TV uses opposite differential directions to make the difference map more sparsity and this prior can be used as a better constraint of images edge than isotropic TV [12]. The anisotropic TV norm of image x is defined as:

$$||x||_{TV} = \sum\nolimits_i ||D_p x||_1 = \sum\nolimits_i (|D_p^h x| + |D_p^v x|)$$

where D_p^h and D_p^v denote finite difference approximations to the partial derivatives of x at the pixel p along the horizontal and vertical direction. Then p will iterate through all the pixels in the image x.

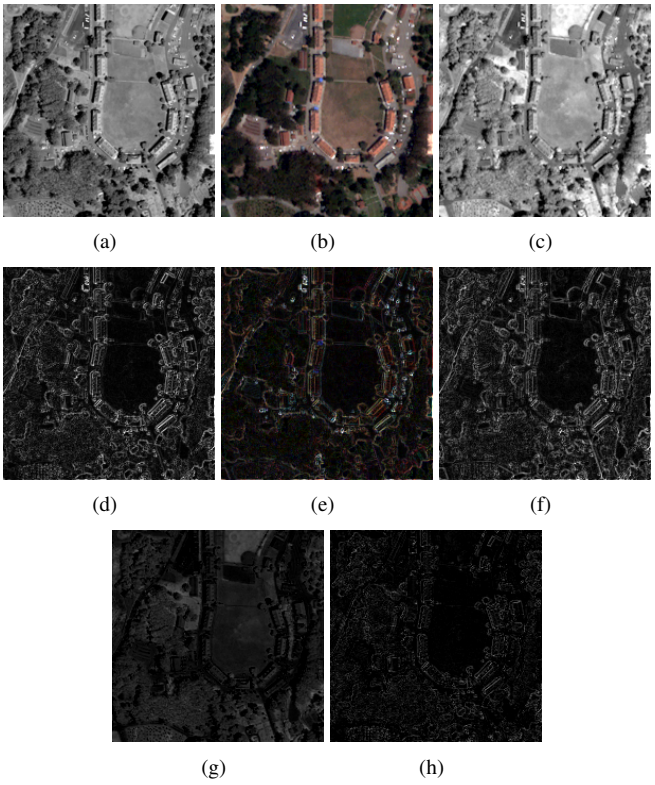

Fig. 1. QuickBird. (a) PAN image. (b) Original HRMS image (RGB). (c) Original near-infrared (NIR) image. (d)Gradient of PAN image. (e) Gradient of HRMS image (RGB). (f) Gradient of near-infrared (NIR) image. (g) The residual image between PAN image and HRMS images ($\omega_1 = \omega_2 = \omega_3 = \omega_4 = 0.25$). (h) The residual gradient of PAN image and HRMS images ($\omega_1 = \omega_2 = \omega_3 = \omega_4 = 0.25$).

3. ALGORITHM

In order to optimize the objective function given in (1) with respect to x_i, first of all, we need to obtain the blurring kernel k. Since satellites such as IKONOS, QuickBird and Pléiades have their own characteristics, the blurring kernel k obtained from LRMS images is diverse from each other in different satellites. According to this condition, we need to estimate the blurring kernel from different satellites, and once the blurring kernel for each satellite has been estimated, it can remain unchanged. We reference [13] to estimate the blurring kernel by solving the following objective function:

$$\min_{Dx,k} \phi\|k * Dx - Dy^{MS}\|_2^2 + \frac{\|Dx\|_1}{\|Dx\|_2} + \psi\|k\|_1 \qquad (4)$$
$$s.t.\ \ k \geq 0, \sum\nolimits_i k_i = 1$$

The first term denotes that the LRMS images are proximity to the HRMS images in the structural part. The second term is the $l1/l2$ regularizer which encourages the scale-invariant sparsity. The $l1$ regularization on k in order to reduce noise in the kernel [13]. ϕ and ψ are the weight parameters. The detailed solutions can be referred to [13].

Once blurring kernel k has been estimated, we seek an appropriate solver x_i to minimize the objective function given in (1). From the ADMM theory [11], we define the anisotropic TV coefficients as $B_{p,i} := D_p x_i$ and we insert $B_{p,i}$ for $D_p x_i$ in the objective under the constraint that they are equal. Then we split the objective L into two sub-problems respectively.

$$P1 : B_{p,i}^{'} = \arg\min_{B} \frac{\lambda}{2}||B_{p,i}||_2 + \frac{\beta}{2}||D_p x_i - B_{p,i} + \mu_{p,i}||_2^2.$$

$$P2 : x_i^{'} = \arg\min_{x_i} \frac{v_1}{2}\sum_{i=1}^{N} f_1(x_i, y_i^{MS}) + \frac{v_3}{2}\sum_{i=1}^{N} f_3(x_i, y^P) +$$
$$\frac{v_2}{2}\sum_{i=1}^{N-1} f_2(x_i, y_i^{MS}) + \frac{\beta}{2}||D_p x_i - B_{p,i} + \mu_{p,i}||_2^2.$$

$$\mu_{p,i}^{'} = \mu_{p,i} + D_p x_i^{'} - B_{p,i}^{'}.$$

P1 and P2 have a globally optimal and closed form solution, while the update for μ_i follows from ADMM.

1) Algorithm for P1 sub-problem: A generalized shrinkage operation [14] can be used for $B_{p,i}^{'}$ exactly,

$$B_{p,i}^{'} = \max\{||D_p x_i + \mu_{p,i}||_2 - \frac{\lambda}{\beta}, 0\} \cdot \frac{D_p x_i + \mu_{p,i}}{||D_p x_i + \mu_{p,i}||_2}$$

After updating x_i, we update the Lagrange multiplier $\mu_{p,i}^{'} = \mu_{p,i} + D_p x_i^{'} - B_{p,i}^{'}$.

2) Algorithm for P2 sub-problem: It is a least squares problem to reconstruction HRMS images for each spectral band, and it has a closed form solution that satisfies

$$[v_1 K^T K + v_2(N-i) + v_3\omega_i^2 G^T G + \beta D^T D]x_i$$
$$= v_1 K^T y_i^{MS} + v_2 \sum_{n=i+1}^{N} |x_n - y_n^{MS} + y_i^{MS}|$$
$$+ v_3\omega_i G^T G(y^P - \sum_{b\neq i}\omega_b x_b) + \beta D^T(B_i - u_i) \qquad (5)$$

We replace the blurring kernel k by the blurring matrix K for convenient writing in (4). The solution x_i is obtained by working within Fourier space. We present x_i by its Fourier coefficients $\theta_i = Fx_i$, where F denotes the Fourier matrix. The diagonal matrix $\Lambda_{1,i}$, contains the unique eigenvalues of the different circulant matrix $K^T K$. The matrix $G^T G$ equals to $D^T D$ since it is a spatial finite difference matrix, they share common eigenvalues $\Lambda_{2,i}$.

$$\theta_i = F(v_1 K^T y_i^{MS} + v_2 \sum_{n=i+1}^{N} |x_n - y_n^{MS} + y_i^{MS}| +$$
$$v_3\omega_i G^T G(y^P - \sum_{b\neq i}\omega_b x_b) + \beta D^T(B_i - u_i))/$$
$$v_1\Lambda_{1,i} + (v_3\omega_i^2 + \beta)\Lambda_{2,i} + v_2(N-i) \qquad (6)$$

Then, we invert θ_i via the inverse Fourier transform to obtain the reconstruction x_i for spectral band i.

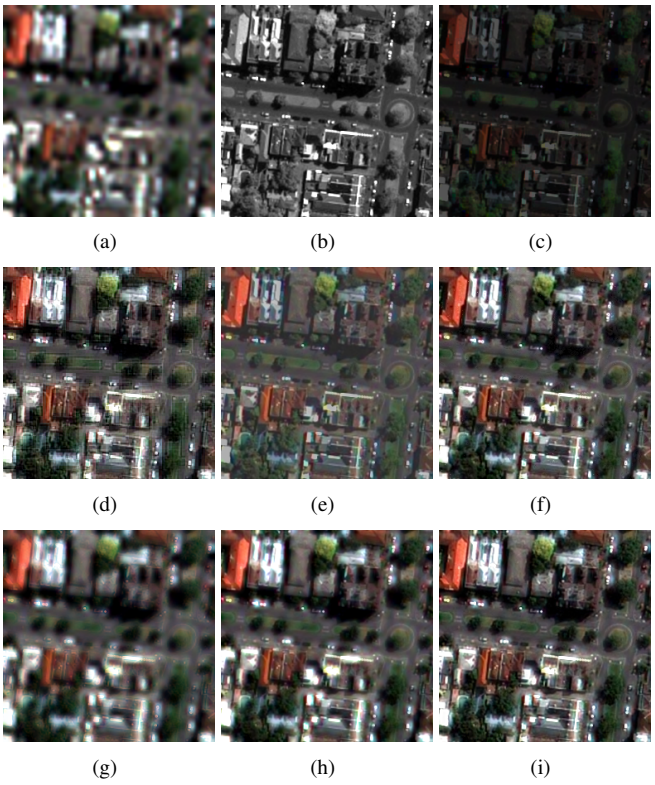

Fig. 2. Pléiades images and pan-sharpening results by different approaches. (a) LRMS images. (b) PAN image. (c) Brovey. (d) Wavelet. (e) PCA. (f) Adaptive IHS. (g) Guided-filter. (h) BPFA. (i) Proposed

4. EXPERIMENTAL RESULTS AND COMPARISONS

4.1. Data sets

The data set from the Pléiades satellite contains a PAN image with 0.5-m resolution and four spectral bands, R, G, B and NIR with 2-m resolution. The dimension of the PAN image is 256×256 and the dimension of each spectral band is 64×64.

4.2. Experimental Strategies and Model Parameters

In our experiments, after using the blind deconvolution algorithm to estimate the blurring kernel for size 7×7, we compare with other well-known approaches such as wavelet-based image fusion [15], PCA-based method [3], Brovey [4], Adaptive IHS [6], Guided-filter based method [10] and BPFA method [8]. Since there is no ground truth for quantitative assessments, we down-sampled the original data to a lower resolution. Then, the original LRMS images are considered as the true references to be compared with the obtained results. In addition, the LRMS images are re-sampled to the same size as the PAN image when pan-sharpening process is carried out. The parameters $\omega_1, \omega_2, \omega_3$ and ω_4 are all to be set the same value as 0.25. We set $v_1 = 5$, $v_2 = 10$, $v_3 = 0.02$, $\lambda = 0.06$ and the ADMM parameter $\beta = 50$.

Table 1. Quality metrics of different methods on Pléiades images from Fig. 2.

	RMSE	CC	ERGAS	Q4
Brovey [4]	0.2741	0.7907	65.5218	0.2519
Wavelet [16]	0.1102	0.8767	8.3039	0.7936
PCA [3]	0.1444	0.8302	11.0561	0.6349
Adaptive IHS [6]	0.1090	0.9012	8.2228	0.7713
BPFA [8]	0.1027	0.8980	7.7802	0.8353
Guided-filter [10]	0.1212	0.8491	9.1618	0.6826
3×3 average	0.1016	0.8954	7.6677	0.7909
Ours	**0.0945**	**0.9103**	**7.1189**	**0.8396**
Ours w/o G_i	0.1056	0.8934	7.5846	0.8129

Figure 2(c)-(i) show the pan-sharpening results for different algorithm on the Pléiades image. By visually comparison, several methods demonstrate clear edges, but they exhibit a visible spectral distortion.

Usually, the spectral quality and the spatial quality are both important, and the spectral quality is more difficult to judge visually. Therefore we quantitatively evaluate the reconstructions using the following metrics: Correlation coefficient (CC), Rootmean-square error (RMSE), *erreur relative global adimensionnelle de synthése* (ERGAS) and Q4 [16].

The quantitative results are shown in Tab. 1 and we highlight the best result in bold. In the table, we also show the results which replace G_i with the identity matrix in the third data fidelity term. We can notice an improvement to our method of focusing on the high-frequency edge within the PAN image and allowing the spectral information to come only from the LRMS images. We also see an advantage to our blurring kernel estimation by comparing with other methods which apply the widely used 3×3 average blurring kernel for pan-sharpening. In general, the anisotropic TV has a positive impact as well.

5. CONCLUSION

We proposed a new CS-based pan-sharpening method which contains joint data fidelity and a novel anisotropic TV. The joint data fidelity focus on the fidelity between HRMS images and LRMS images, HRMS images and PAN image in high frequency part, the gradient of HRMS images and LRMS images in the spectrum direction. The novel anisotropic TV helps to enforce the edges of HRMS images. We introduce a blind deconvolution algorithm to estimate the blurring kernel from different satellites adaptively. What's more, the alternating direction method of multipliers (ADMM) helps to perform our method efficient. By comparing with the other well-known methods, our experiment results on Pléiades image shows that the proposed approach gives both higher spatial and spectral resolution.

6. REFERENCES

[1] M.V. Joshi, L. Bruzzone, and S. Chaudhuri, "A model-based approach to multiresolution fusion in remotely sensed images," *IEEE Trans. Geosci.Remote Sens.*, vol. 44, no. 9, pp. 2549–2562, Sep 2006.

[2] S. Li and B Yang, "A new pansharpening method using a compressed sensing technique," *IEEE Trans. Geosci.Remote Sens.*, vol. 49, no. 2, pp. 738–746, Feb 2011.

[3] V. P. Shah, N. H. Younan, and R. L. King, "An efficient pan-shapening method via a combined adaptive pca approach and contourlets," *IEEE Trans. Geosci.Remote Sens.*, vol. 46, no. 5, pp. 1323–1335, May 2008.

[4] A. Eshtehardi, H. Ebadi, Z. Valadan, and A. Mohammmadzadeh, "Image fusion of landsat etm+ and spot satellite images using ihs, brovey and pca," in *Conference on information extraction from SAR and optical data, with emphasis on developing countries*, 2007.

[5] H. Aanæs and J. Sveinsson, "Model-based satellite image fusion," *IEEE Trans. Geosci.Remote Sens.*, vol. 46, no. 5, pp. 1336–1346, May 2008.

[6] S. Rahmani, M. Strait, D. Merkurjev, M. Moeller, and T. Wittman, "An adaptive ihs pansharpening method," *IEEE Trans. Geosci.Remote Sens.*, vol. 7, no. 4, pp. 746–750, Oct 2010.

[7] X. X. Zhu and R. Bamler, "A sparse image fusion algorithm with application to pansharpening," *IEEE Trans. Geosci.Remote Sens.*, vol. 51, no. 5, pp. 2827–2836, 2013.

[8] J. Xie, Y. Huang, J. Paisley, X. H. Ding, and X. P. Zhang, "Pan-sharpening based on nonparametric bayesian adaptive dictionary learing," in *ICIP*, 2013.

[9] X. X. Zhu and R Bamler, "A sparse image fusion algorithm with application to pansharpening," *IEEE Trans. Geosci.Remote Sens.*, vol. 51, no. 5, pp. 2827–2836, 2013.

[10] F. Fang, F. Li, C. Shen, and Zhang, "A variational approach for pan-sharpening," *IEEE Transactions on Image Processing.*, vol. 22, no. 7, pp. 2822–2834, July 2013.

[11] Parikh N. Chu E. Peleato B. Boyd, S. and J. Eckstein, "Distributed optimization and statistical learning via the alternating direction method of multipliers," *Foundations and Trends in Machine Learning*, vol. 3, no. 1, pp. 1–122, 2011.

[12] M. Grasmair and F. Lenzen, "Anisotropic total variation filtering," *Applied Mathematics & Optimization*, vol. 62(3), 2010.

[13] Tay T. Krishnan, D. and R. Fergus, "Blind deconvolution using a normalized sparsity measure," *Computer Vision and Pattern Recognition (CVPR)*, 2011.

[14] T. Goldstein and S Osher, "The split bregman method for l1-regularized problems," *SIAM J. imaging Sci.*, vol. 2, no. 2, pp. 323–343, 2009.

[15] X. Otazu and Gonzalez-Audicana, "Introduction of sensor spectral response into image fusion methods: Application to wavelet-based methods," *IEEE Trans. Geosci.Remote Sens.*, vol. 43, no. 10, pp. 2376–2385, 2005.

[16] Z. Wang and A. C. Bovik, "A universal image quality index," *IEEE Trans. Geosci.Remote Sens.*, vol. 9(3), pp. 81–84, 2002.